

## MIT Open Access Articles

*Plant Nanobionic Sensors for Arsenic Detection*

The MIT Faculty has made this article openly available. **Please share** how this access benefits you. Your story matters.

**Citation:** Lew, Tedrick Thomas Salim, Park, Minkyung, Cui, Jianqiao and Strano, Michael S. 2020. "Plant Nanobionic Sensors for Arsenic Detection." *Advanced Materials*, 33 (1).

**As Published:** <http://dx.doi.org/10.1002/adma.202005683>

**Publisher:** Wiley

**Persistent URL:** <https://hdl.handle.net/1721.1/140521>

**Version:** Author's final manuscript: final author's manuscript post peer review, without publisher's formatting or copy editing

**Terms of use:** Creative Commons Attribution-Noncommercial-Share Alike



1 Plant Nanobionic Sensors for Arsenic Detection

2 Tedrick Thomas Salim Lew<sup>1</sup>, Minkyung Park<sup>1</sup>, Jianqiao Cui<sup>1</sup> and Michael S. Strano<sup>1,\*</sup>

3 <sup>1</sup>Department of Chemical Engineering, Massachusetts Institute of Technology, 77 Massachusetts  
4 Avenue, Cambridge, MA 02139, USA

5 \*Corresponding author's email address: [strano@mit.edu](mailto:strano@mit.edu)

## 6 ABSTRACT

7 Arsenic is a highly toxic heavy metal pollutant which poses a significant health risk to  
8 humans and other ecosystems. In this work, the natural ability of wild-type plants to pre-  
9 concentrate and extract arsenic from the belowground environment is exploited to engineer plant  
10 nanobionic sensors for real-time arsenic detection. Near-infrared (NIR) fluorescent nanosensors  
11 were specifically designed for sensitive and selective detection of arsenite. These optical  
12 nanosensors were embedded in plant tissues to non-destructively access and monitor the internal  
13 dynamics of arsenic taken up by the plants via the roots. The integration of optical nanosensors with  
14 living plants enabled the conversion of plants into self-powered autosamplers of arsenic from their  
15 environment. Arsenite detection was demonstrated with three different plant species as nanobionic  
16 sensors. Based on an experimentally-validated kinetic model, the nanobionic sensor could detect 0.6  
17 ppb and 0.2 ppb levels of arsenic after 7 and 14 days respectively by exploiting the natural ability of  
18 *Pteris cretica* ferns to hyperaccumulate and tolerate exceptionally high level of arsenic. The sensor  
19 readout could also be interfaced with portable electronics at a standoff distance, potentially  
20 enabling applications in environmental monitoring and agronomic research.

21 **Keywords:** plant nanobionic, optical sensor, carbon nanotube, arsenic, nanoparticles, molecular  
22 recognition

23

This is the author manuscript accepted for publication and has undergone full peer review but has not been through the copyediting, typesetting, pagination and proofreading process, which may lead to differences between this version and the [Version of Record](#). Please cite this article as [doi: 10.1002/adma.202005683](https://doi.org/10.1002/adma.202005683).

This article is protected by copyright. All rights reserved.

24 **MAIN TEXT**

25 The abundance of arsenic compounds in the environment poses a serious threat to human health  
26 and ecosystems.<sup>[1,2]</sup> Long-term exposure to arsenic in humans is associated with cardiovascular  
27 diseases, birth defects, severe skin lesions and various types of cancer.<sup>[3,4]</sup> Anthropogenic activities  
28 such as mining, smelting, irrigation with arsenic-contaminated water and the extensive use of  
29 arsenic-based pesticides in the past decades have led to significant arsenic accumulation in  
30 underground water and agricultural soils.<sup>[5-7]</sup> Elevated levels of arsenic in the soils not only inhibit  
31 plant growth and result in substantial losses in crop production, but also lead to higher arsenic  
32 uptake by crops and contamination of the food chain.<sup>[7-9]</sup> These concerns over arsenic exposure  
33 prompted the World Health Organization (WHO) and Food and Agriculture Organization (FAO) of the  
34 United Nations to set the maximum contaminant level of arsenic in drinking and irrigation water to  
35 10 ppb and 100 ppb respectively.<sup>[10]</sup>

36 Arsenic exists primarily as arsenite ( $\text{As}^{3+}$ ) and arsenate ( $\text{As}^{5+}$ ) in aqueous environment.<sup>[11]</sup> In  
37 anaerobic conditions such as paddy soils, arsenite is the predominant chemical form of arsenic and it  
38 can be efficiently taken up by plants via different mechanisms.<sup>[12,13]</sup> However, there is a lack of  
39 reliable techniques capable of rapidly assessing the uptake of arsenic in plants or the arsenic content  
40 within agricultural soil. The conventional method to determine the arsenic level in plants and soil is  
41 based on regular field sampling, plant tissue digestion, extraction and analysis using mass  
42 spectrometry.<sup>[14-17]</sup> Such sampling procedure requires extensive sample pre-treatment, bulky and  
43 expensive instrumentation, and does not allow for real-time monitoring of arsenic contamination in  
44 the field.<sup>[18]</sup> Reflectance spectroscopy and hyperspectral imaging have been proposed as alternatives  
45 to monitor arsenic level in plants at a remote distance.<sup>[19-21]</sup> However, these methods are non-  
46 specific towards arsenic contamination, and they rely on slow phenotypic changes of stressed plants  
47 such as significant reduction in chlorophyll concentration, destruction of leaf cellular structure and  
48 appearance of chlorotic symptoms.<sup>[19,22]</sup> Electrochemical and optical arsenic detection using  
49 nanoparticles have been demonstrated *in-vitro* and in contaminated water samples,<sup>[23-27]</sup> but their  
50 application to monitor the arsenic uptake within plants in real time remains unexplored.

51 In this work, we demonstrate the use of living plants, interfaced with specifically designed  
52 nanomaterials, to serve as self-powered and naturally occurring detectors of arsenic present in  
53 belowground environment. This plant nanobionic approach enables real-time monitoring of arsenite  
54 taken up by the roots of wild-type plants at a standoff distance. A pair of SWNT-based NIR  
55 fluorescent nanosensors was rationally designed to selectively recognize arsenite via modulation of  
56 their emission intensity. These nanosensors were embedded in the leaf mesophyll of living plants,  
57 enabling the detection of arsenite molecules as they are taken up by the roots, transported along  
58 the plant vasculature and pre-concentrated in the leaf lamina. The integration of our nanosensors  
59 with Cretan brake fern (*Pteris cretica*), a fern species capable of hyperaccumulating high levels of  
60 arsenic in their tissues, enabled the standoff detection of arsenite at the low ppb level, well below  
61 the regulatory limit of arsenic in drinking and irrigation water. By harnessing the unique optical  
62 properties of nanomaterials and the natural properties of plants to pre-concentrate and  
63 hyperaccumulate arsenic, we show the engineering of living plants as autonomous microfluidic

64 samplers capable of real-time, non-destructive and ultrasensitive detection of arsenite in the  
65 environment.

66

## 67 **Nanosensor development and characterization**

68 Herein, we use the corona phase molecular recognition (CoPhMoRe) technique, which we  
69 have previously introduced,<sup>[28]</sup> to develop SWNT-based optical nanosensors for selective detection of  
70 arsenite. In this technique, an adsorbed heteropolymer phase on the SWNT surface, called the  
71 corona, provides synthetic molecular recognition sites that can bind or interact with the target  
72 analyte. Such interaction translates into modulations in the NIR fluorescence spectrum of SWNT, and  
73 enables the detection of a variety of target analytes including small signaling molecules and  
74 nitroaromatic compounds in living plants.<sup>[29–31]</sup> SWNT offers unique advantages for long-term  
75 sensing applications *in planta* because they fluoresce in the near-infrared region away from the  
76 chlorophyll autofluorescence and do not photobleach.<sup>[32,33]</sup> In addition, their surface properties can  
77 be engineered to target different plant organs or subcellular organelles.<sup>[34–36]</sup>

78 Arsenite is chosen as the target analyte because it is the predominant form of arsenic in  
79 anaerobic paddy soils which can be taken up efficiently by crops through silicon transporters in the  
80 roots.<sup>[12,37,38]</sup> Previous studies have shown that guanine (G) and thymine (T) nucleotides can form  
81 strong hydrogen bonds with the hydroxy (-OH) groups of arsenite.<sup>[39,40]</sup> To exploit the ability of  
82 certain DNA bases to interact with arsenite, we first constructed a library of single stranded DNA  
83 (ssDNA)-wrapped SWNT with oligonucleotides of varying lengths and G-/T- compositions. The optical  
84 sensor responses of DNA-wrapped SWNT constructs were recorded following a 15-minute  
85 incubation of 100  $\mu\text{M}$  arsenite in 0.1 M NaCl solution buffer. SWNT wrapped with oligonucleotide  
86 sequences containing high G-/T- content, such as  $(\text{GT})_N$ -SWNT where  $N = 5$  to 30, exhibit a significant  
87 increase in fluorescence intensity ( $(I-I_0)/I_0$ ) by as much as 650% for the (9,4) SWNT chirality upon the  
88 addition of arsenite (**Figure 1a**). Substitution of G-/T- nucleotides with adenine (A) or cytosine (C),  
89 such as  $(\text{GTAA})_7$ -SWNT and  $(\text{GTCC})_7$ -SWNT, diminishes the DNA-SWNT sensor response towards  
90 arsenite. Oligonucleotide sequences which do not contain G-/T- bases, such as  $\text{C}_{30}$ -SWNT and  $(\text{AC})_{15}$ -  
91 SWNT, remain largely nonresponsive when exposed to arsenite (**Figure 1a**). The decrease in sensor  
92 sensitivity as the G-/T- composition in the corona phase is reduced confirms previous findings which  
93 show that G-/T- nucleotides are potential binding sites with arsenite.<sup>[39,40]</sup> In addition, we found that  
94 the oligonucleotide length of the  $(\text{GT})_N$ -SWNT construct significantly affected the fluorescence  
95 intensity modulation from arsenite. Shorter  $(\text{GT})_N$  polymers yield higher intensity change in response  
96 to arsenite compared to longer  $(\text{GT})_N$  sequences, with  $(\text{GT})_5$ -SWNT and  $(\text{GT})_{25}$ -SWNT showing a  
97 maximum and minimum response of 650% and 210% respectively.  $(\text{GT})_N$  sequences for  $N < 5$  were  
98 not investigated due to the apparent instability of these DNA-SWNT constructs which would hinder  
99 their *in planta* sensing applications.<sup>[41]</sup> Since G and T nucleobases also strongly pi-stack onto the  
100 SWNT surface,<sup>[42]</sup> the length dependence suggests a trade-off between arsenite and SWNT surface  
101 binding that is optimized at  $N = 5$ .

102 Nanosensor responses towards arsenate were also evaluated to investigate the selectivity of  
103 DNA-SWNT constructs in distinguishing different arsenic species. In comparison to the sensitivity of  
104 the nanosensors towards arsenite, the modulation of DNA-SWNT fluorescence intensity was smaller  
105 upon the addition of 100  $\mu\text{M}$  arsenate for all DNA-SWNT hybrids tested in this study (**Figure 1b**).  
106 Among  $(\text{GT})_{\text{N}}$ -SWNT,  $(\text{GT})_5$ -SWNT shows the minimal turn-on response of 15% while  $(\text{GT})_{30}$ -SWNT  
107 shows a 110% response towards arsenate. The weaker response of  $(\text{GT})_{\text{N}}$ -SWNT elicited by arsenate  
108 compared to arsenite may be attributed to the presence of ketone group in arsenate, which can  
109 disrupt the formation of hydrogen bonds with the amine groups of G-/T- nucleotides.<sup>[43]</sup> As  $(\text{GT})_5$ -  
110 SWNT shows the highest sensitivity and selectivity towards arsenite, we further investigated if such  
111 sensor performance is unique to  $(\text{GT})_5$  sequence or if other short 10-mer sequences also exhibit  
112 similar sensitivity. We found that substitution of G-/T- bases with C nucleotides, which have a high  
113 affinity to bind onto SWNT sidewall,<sup>[44,45]</sup> decreased the sensor sensitivity towards arsenite (**Figure**  
114 **S1, Supporting Information**). This is similar to the trend observed among longer oligonucleotide  
115 sequences and suggests that the specific oligonucleotide chemistry is responsible for the sensor  
116 sensitivity and selectivity (**Figure 1a**).

117 The large intensity increase of  $(\text{GT})_5$ -SWNT observed upon arsenite interaction can be  
118 attributed to the low baseline fluorescence of SWNT chiralities with larger diameter (**Figure 1c**). The  
119 excitation-emission map of  $(\text{GT})_5$ -SWNT also confirmed that the largest intensity modulations  
120 induced by arsenite were exhibited by large-diameter SWNT chiralities (**Figure S2, Supporting**  
121 **Information**). Recent studies suggested that short  $(\text{GT})_6$  polymers form highly-ordered ring  
122 structures on the SWNT surface, creating a periodic charge distribution which effectively provides an  
123 effective doping of SWNT.<sup>[41]</sup> This doping effect suppresses the radiative exciton relaxation and  
124 activates nonradiative exciton relaxation mechanisms, giving rise to the quenched baseline  
125 fluorescence of short  $(\text{GT})_{\text{N}}$ -SWNT constructs. The corona structure of adsorbed DNA on the SWNT  
126 surface is influenced by the solution microenvironment such as ionic strength and pH.<sup>[46]</sup> Thus, we  
127 further tested the response of  $(\text{GT})_{\text{N}}$ -SWNT nanosensors in MES and TES buffers which are commonly  
128 used for plant infiltration.<sup>[31,47]</sup>  $(\text{GT})_{\text{N}}$ -SWNT constructs maintain their turn-on response upon arsenite  
129 exposure, with  $(\text{GT})_5$ -SWNT exhibiting the highest sensitivity of 218% and 195% in MES and TES  
130 buffer respectively (**Figure S3, Supporting Information**). The responses of  $(\text{GT})_5$ -SWNT against  
131 different concentrations of arsenite could be fitted to a kinetic adsorption model to yield a sensor  
132 dissociation constant ( $K_d$ ) of 26  $\mu\text{M}$  (**Figure 1d**).<sup>[48]</sup> The limit of detection of  $(\text{GT})_5$ -SWNT, calculated  
133 from the arsenite concentration which resulted in a signal-to-background ratio  $\geq 3$ , was estimated to  
134 be 122 nM. In addition, the  $(\text{GT})_5$ -SWNT sensor response towards arsenite can be reversed with the  
135 introduction of ethylenediaminetetraacetic acid (EDTA), a common metal chelating agent (**Figure S4,**  
136 **Supporting Information**).  $(\text{GT})_5$ -SWNT complexes were also selective towards arsenite over other  
137 heavy metal ions which may be present as contaminants in the soil (**Figure 1e**). Taken together, the  
138 high sensitivity, selectivity and compatibility in biologically relevant environment motivates the  
139 application of  $(\text{GT})_5$ -SWNT to probe arsenite level *in planta*.

140 **Integration of optical nanosensors with living plants**

141 Spinach plants (*Spinacia oleracea*) were turned into an autonomous detector of arsenite by  
142 interfacing with a SWNT-based ratiometric sensor platform consisting of a reference and an active  
143 sensor. In this platform, (GT)<sub>5</sub>-SWNT served as the active sensor which would exhibit a turn-on  
144 response upon arsenite detection, while C<sub>10</sub>-SWNT was selected as the reference sensor which  
145 would remain invariant upon arsenite exposure. The DNA-SWNT constructs were infiltrated into two  
146 different regions of a leaf lamina of spinach plants, separated by the midrib, via syringe infiltration at  
147 the adaxial side (**Figure 2a**). Arsenite solution was then introduced to the root environment and as  
148 transpiration occurs, arsenite would be taken up by the roots and transported to the leaf via the  
149 plant vasculature where they would eventually accumulate and come into contact with the  
150 embedded nanosensors. The NIR fluorescence of both sensor complexes were monitored at a  
151 standoff distance of 1 m with a two-dimensional (2D) array InGaAs detector. (GT)<sub>5</sub>-SWNT  
152 fluorescence intensity started to increase approximately 30 minutes after the introduction of 10 μM  
153 arsenite solution to the roots of spinach plants (**Figure 2b**). After 5 hours, an 11% increase in the  
154 average (GT)<sub>5</sub>-SWNT fluorescence intensity was observed – this intensity modulation corresponds to  
155 approximately 0.3 μM change in leaf arsenite concentration (**Figure 2c**). In contrast, the fluorescence  
156 intensity of the control sensor, C<sub>10</sub>-SWNT, remained relatively invariant throughout the experiment  
157 as expected. The relative intensity of (GT)<sub>5</sub>-SWNT to C<sub>10</sub>-SWNT ( $I_{G/C-SWNT}$ ) was defined as the readout  
158 of the ratiometric sensor approach. When water was introduced to the roots of spinach plants as a  
159 control,  $I_{G/C-SWNT}$  remained relatively constant over 5 hours (**Figure 2d**). The difference in the  
160 responses of the nanosensors confirmed that our ratiometric platform enabled the selective  
161 detection of arsenite as they were taken up by the roots and transported to the leaf lamina. The  
162 embedded nanosensors could tap into plants' internal state and allow the interfacing of such  
163 information to electronics, enabling plants to serve as nanobionic devices which can communicate  
164 the information they receive from the environment to detectors easily interpreted by human.

165 The nanobionic approach can also be extended to other plant species to convert any wild-  
166 type plants into arsenic detectors. The nanosensor platform was applied to monitor arsenic uptake  
167 in rice plants (*Oryza sativa*). As a staple food for half of the global human population, rice is a major  
168 dietary source of arsenic.<sup>[49,50]</sup> Previous reports have shown that rice accumulates arsenite more  
169 efficiently than other cereal crops such as barley (*Hordeum vulgare*) or wheat (*Triticum aestivum*),  
170 elevating the concerns of arsenic contamination of the human food chain.<sup>[51,52]</sup> The introduction of  
171 10 μM arsenite to the roots of 6-week old rice plants resulted in an average of 15% increase in the  
172  $I_{G/C-SWNT}$  profile after 5 hours (**Figure 2e, f**). The  $I_{G/C-SWNT}$  level remained relatively constant in the  
173 absence of arsenite. The variance in the sensor response dynamics between rice and spinach plants  
174 may be due to differences in biological factors such as the vascular structure between  
175 monocotyledonous (e.g. rice) and dicotyledonous plants (e.g. spinach), distribution of arsenic uptake  
176 channels in the roots, as well as the leaf surface area which affects the transpiration rate.  
177 Nonetheless, these results suggest that the nanosensors can be applied to probe the arsenite uptake  
178 in both monocotyledonous and dicotyledonous plant species, such as rice and spinach respectively.  
179 This provides a unique practical advantage in contrast to genetic engineering methods to produce  
180 biosensors for analyte detection *in planta*, which are only feasible in a limited number of plant  
181 species.<sup>[33]</sup>

## 182 Arsenic detection with nanosensors in the visible range

183 We further demonstrated the versatility of our nanosensor probe for imaging in both the NIR range  
184 as well as the visible spectra. To enable imaging of the probe in the visible region, we prepared self-  
185 assembled nanostructures comprising of SWNT, single-stranded (GT)<sub>5</sub> sequence and TO-PRO-1 (TP),  
186 a cyanine dye that intercalates with DNA. Unlike common fluorescent dyes which are typically  
187 quenched in the proximity of SWNT, TP switches from a non-fluorescent state to a highly fluorescent  
188 state when constrained in a conformationally restrictive environment.<sup>[53]</sup> Upon tip-sonication, the  
189 three components readily self-assemble to form TP-(GT)<sub>5</sub>-SWNT nanoconstructs which are  
190 fluorescent in both the NIR range, enabled by the SWNT backbone, and the visible range, enabled by  
191 the TP dye. Successful incorporation of TP into the (GT)<sub>5</sub>-SWNT construct was confirmed the  
192 appearance of a distinct absorption peak at 515 nm in TP-(GT)<sub>5</sub>-SWNT absorbance spectrum, which  
193 corresponds to the absorption maximum of TP dye (**Figure 3a**). TP-(GT)<sub>5</sub>-SWNT still maintain well-  
194 defined NIR fluorescence profile and, more importantly, the nanoconstructs show similar intensity  
195 modulation towards arsenite with and without TP intercalation (**Figure 3b**). Additionally, the  
196 fluorescence of TP-(GT)<sub>5</sub>-SWNT in the visible range decreases in response to arsenite with a  
197 comparable sensitivity range as that of (GT)<sub>5</sub>-SWNT in the NIR range (**Figure 3c**). To determine if this  
198 intensity modulation in the visible region is caused by the specific interaction between arsenite and  
199 (GT)<sub>5</sub> sequences, we also prepared TP-C<sub>10</sub>-SWNT and monitored its response towards arsenite. The  
200 fluorescence of TP-C<sub>10</sub>-SWNT in the visible range remained unaffected upon the introduction of  
201 arsenite at different concentrations (**Figure 3c**). These findings suggest that the interaction between  
202 the (GT)<sub>5</sub> wrapping and arsenite may induce a conformational change in the SWNT corona phase and  
203 the bound TP molecules, leading to intensity modulation of the dye-labelled nanoconstructs.

204 The nanosensors' visible fluorescence enables the visualization of nanosensor dynamics  
205 within plant cells at a subcellular resolution with visible confocal microscopy. TP-(GT)<sub>5</sub>-SWNT  
206 complexes are localized along the cell membrane in the spinach mesophyll layer after syringe  
207 infiltration to the adaxial side of a spinach leaf (**Figure 3d**). As shown in Figure 3d, the addition of 10  
208 μM arsenite decreases the visible fluorescence intensity of the nanocomplexes with different  
209 magnitude at various subcellular locations. Three randomly-selected locations of TP-(GT)<sub>5</sub>-SWNT  
210 showed quenching magnitudes between 30 and 60% (**Figure 3e**). The heterogeneous sensor  
211 dynamics between different subcellular locations may be caused by the spatial profile of arsenite  
212 transport within plant cells, or the distribution of nanosensors within the leaf mesophyll. This  
213 demonstration highlights the facile modification that can be employed to engineer versatile SWNT-  
214 based probes, allowing application in the NIR range for whole plant imaging as well as in the visible  
215 region for subcellular arsenite detection as shown in this work.

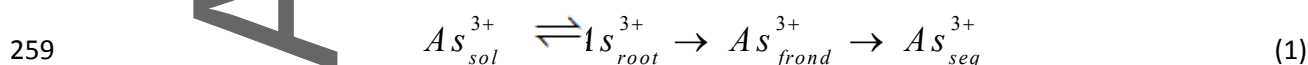
## 216 Nanobionic sensors based on arsenic hyperaccumulators

217 Plants exhibit natural diversity in their adaptive responses to thrive in arsenic-containing  
218 soils. Some species of plants, primarily ferns from the *Pteris* genus, have naturally evolved the  
219 exceptional capability to accumulate and tolerate a high concentration of arsenic in their  
220 aboveground biomass.<sup>[54-56]</sup> For example, the Chinese brake fern *Pteris vittata*, the first known  
221 arsenic hyperaccumulating fern, can concentrate as much as 5,131 ppm arsenic in the fronds when

222 grown in soil containing 50 ppm arsenic over 2 weeks.<sup>[57]</sup> In this work, we harnessed the  
 223 hyperaccumulating capability of the Cretan brake fern *P. cretica*, a previously identified arsenic  
 224 hyperaccumulator,<sup>[54,58]</sup> to enhance the sensitivity of plant nanobionic sensors for arsenic detection.  
 225 Both (GT)<sub>5</sub>-SWNT and C<sub>10</sub>-SWNT were applied on separate sides of the costa, the midrib of the fern  
 226 leaflet (**Figure 4a**). Upon exposure to 10 μM arsenite solution at the roots, the NIR fluorescence  
 227 intensity of (GT)<sub>5</sub>-SWNT showed a steady increase over 7 days relative to the initial value, while that  
 228 of C<sub>10</sub>-SWNT remained relatively invariant (**Figure 4b**). The ratiometric sensor response ( $\Delta I/I_0$ ) of *P.*  
 229 *cretica* plants is consistently higher throughout the 7-day period than that of spinach or rice plants,  
 230 showing a significant increase of 74% relative to the initial level. (**Figure 4c**). There was no significant  
 231 difference in the chlorophyll concentration between plants infiltrated with MES buffer and plants  
 232 treated with DNA-SWNT and 10 μM arsenite over the 7-day period (**Figure S5, Supporting**  
 233 **Information**). Inductively coupled plasma mass spectroscopy (ICP-MS) analysis was also performed  
 234 on the treated plant samples to construct a calibration curve which allows the translation of sensor  
 235 intensity modulation to actual changes in the frond arsenic concentration (**Figure S6, Supporting**  
 236 **Information**). The nanosensor intensity modulation can also be captured by a portable Raspberry Pi  
 237 platform equipped with a charge-coupled device (CCD) camera, a similar technology to a commercial  
 238 smartphone-based camera (**Figure S7a, Supporting Information**). Analysis of images collected  
 239 through the CCD camera showed a similar ratiometric sensor response as that captured with the  
 240 InGaAs detector with a 64% increase over 7 days (**Figure S7b, Supporting Information**),  
 241 demonstrating the feasibility of interfacing the plant nanobionic sensor with inexpensive, portable  
 242 electronic devices. The plant nanobionic sensor was then treated with lower concentrations of  
 243 arsenite in the root uptake solution down to 0.1 μM. As expected, the arsenic concentration in *P.*  
 244 *cretica* fronds, obtained from monitoring the nanosensor fluorescence intensity, decreased with  
 245 lower arsenite concentrations in the root uptake solution across the 7-day experiment duration  
 246 (**Figure 4d**). We note that there may be slight differences in the sensor response dynamics if arsenite  
 247 is introduced into the soil instead of the root uptake solution, due to factors such as soil porosity,  
 248 tortuosity, and gravimetric water content. Nonetheless, our work demonstrates that plants can be  
 249 engineered as living environmental sensors for sensitive arsenite detection from the belowground  
 250 environment.

### 251 Kinetic model to estimate plant nanobionic sensor detection limit

252 We described the uptake of arsenite in *P. cretica* with a kinetic model to obtain a theoretical  
 253 limit of detection of the plant nanobionic sensor. For arsenite molecules to be detected by the  
 254 nanosensors embedded in the frond, they have to be taken up by transporters in the roots and  
 255 translocated to the frond via the xylem before coming into contact with the nanosensors. At the  
 256 frond, arsenite may be sequestered into the vacuole for long-term storage and detoxification.<sup>[59,60]</sup>  
 257 The exchange of arsenite between these different compartments can be summarized as a series of  
 258 reactions:





260 where  $As_{sol}^{3+}$ ,  $As_{root}^{3+}$ ,  $As_{frond}^{3+}$  and  $As_{seq}^{3+}$  denote the arsenite species present in the uptake  
 261 solution, roots, frond and sequestration compartment respectively. The nanosensor fluorescence  
 262 intensity indicates the level of  $As_{frond}^{3+}$ . In *P. vittata*, another arsenic hyperaccumulating species in  
 263 the *Pteridaceae* family, the transporter-mediated influx of  $As^{3+}$  from the uptake solution into the  
 264 roots ( $As_{sol}^{3+} \rightarrow As_{root}^{3+}$ ) has been shown to follow Michaelis-Menten kinetics, with a maximum net  
 265 influx rate of 8-10  $\mu\text{mol.As g}^{-1}$  root fresh weight (FW)  $\text{h}^{-1}$  at saturating conditions.<sup>[61]</sup> The  
 266 translocation of  $As^{3+}$  from the roots to the fronds ( $As_{root}^{3+} \rightarrow As_{frond}^{3+}$ ) in *P. vittata* is mainly driven by  
 267 transpiration, with a mean transpiration rate of 5-7  $\text{g.H}_2\text{O g}^{-1}$  frond FW  $\text{d}^{-1}$  under normal  
 268 conditions.<sup>[62]</sup> Accounting for the plant biomass used in this study (approximately 23 g root FW and  
 269 15 g frond FW) and the average arsenite concentration in the xylem sap of hyperaccumulators,<sup>[63]</sup> we  
 270 estimated the arsenite root-to-frond translocation rate and the maximum root influx rate to be 29-  
 271 38  $\mu\text{mol.As d}^{-1}$  and 4.3-5.4  $\mu\text{mol.As d}^{-1}$  respectively. We further defined a modified Damköhler  
 272 number ( $Da$ ) as the ratio between the compartmental exchange rates:

$$Da = \frac{\text{root influx rate}}{\text{root-to-frond translocation rate}} \quad (2)$$

275 When  $Da \gg 1$ , the temporal changes of  $As_{frond}^{3+}$  are controlled primarily by the root-to-frond  
 276 translocation rate, while  $Da \ll 1$  indicates that the root influx rate is the rate-determining step. The  
 277  $Da$  for our plant nanobionic system is approximately 0.11 – 0.18, which indicates that the arsenite  
 278 influx from the uptake solution into the roots is the rate-determining step. As such, assuming the  
 279 root uptake follows a Michaelis-Menten kinetic model and the sequestration process ( $As_{frond}^{3+} \rightarrow As_{seq}^{3+}$ ) follows a first-order reaction, the mass balances of  $As_{frond}^{3+}$  and  $As_{sol}^{3+}$  can be  
 280 described with the following ordinary differential equations:

$$\frac{dn_{frond}}{dt} = \frac{FW_{root} I_{max} C_{sol}}{K_m + C_{sol}} - k_d n_{frond} \quad (3)$$

$$\frac{dC_{sol}}{dt} = - \frac{FW_{root} I_{max} C_{sol}}{V_{sol} (K_m + C_{sol})} \quad (4)$$

284 where  $n_{frond}$  denotes the amount of arsenite in the frond,  $FW_{root}$  is the root fresh weight,  $I_{max}$  is  
 285 the maximum net influx rate of arsenite into the roots,  $C_{sol}$  is the arsenite concentration in the  
 286 uptake solution,  $K_m$  is the Michaelis-Menten constant which is an inverse measure of the root  
 287 transporters' affinity towards arsenite, and  $k_d$  is the first-order sequestration rate constant of

288 arsenite in the frond, and  $V_{sol}$  is the uptake volume solution. The proposed kinetic model can  
289 describe changes in *P. cretica* frond arsenite concentration, obtained from the nanosensor intensity  
290 profile, upon exposure to 10, 5, 1 and 0.1  $\mu\text{M}$  arsenite at the roots with high fidelity (**Figure 4d**). The  
291 fitting process yields three kinetic parameters for the *P. cretica* nanobionic system:  $K_m$  of  $5.84 \pm$   
292  $1.63 \mu\text{M}$ ,  $I_{max}$  of  $3.65 \pm 1.02 \text{ nmol g}^{-1} \text{ root FW h}^{-1}$ , and  $k_d$  of  $0.0012 \pm 0.0004 \text{ h}^{-1}$ . The  $K_m$  value  
293 estimated from our kinetic data is similar to those obtained for *P. vittata* plants previously reported  
294 by other groups (**Table 1**). It is approximately 30 times lower than the  $K_m$  of arsenite transporters  
295 in rice roots ( $180 \mu\text{M}$ ),<sup>[64]</sup> indicating a higher affinity of *P. cretica* roots than rice roots towards  
296 arsenite. The lower value of  $I_{max}$  to that of *P. vittata* indicates a slightly slower arsenite net uptake  
297 rate into the roots of *P. cretica* than *P. vittata*. The low value of  $k_d$  suggests that while the  
298 nanosensor detection mechanism is reversible, *P. cretica* hyperaccumulator takes up arsenite almost  
299 irreversibly and the arsenite detection by plant nanobionic can therefore be considered irreversible.

300 The proposed kinetic model can be used to predict the arsenite concentration in the frond as  
301 a function of plant root biomass, uptake solution volume and uptake duration (**Figure S8, Supporting**  
302 **Information**). We further utilized the model to estimate the theoretical detection limit of *P. cretica*-  
303 based nanobionic arsenite sensor, defined as the minimum arsenite concentration in the root uptake  
304 solution that can be detected by the plant nanobionic sensor. The minimum frond arsenite  
305 concentration that gave a signal-to-background ratio  $\geq 3$  was determined to be  $110 \text{ nmol g}^{-1}$  frond  
306 dry weight (DW). The kinetic model was then utilized to compute the limit of detection in the uptake  
307 solution that results in this level of arsenite in the frond under different experimental conditions and  
308 root biomass. Considering an uptake period of 7 days, a limit of detection of  $4.7 \text{ nM}$  ( $0.6 \text{ ppb}$ ) could  
309 be achieved with roots of  $30 \text{ g FW}$  and uptake solution volume of  $5 \text{ L}$  (**Figure 4e**). This detection limit  
310 suggests that the plant nanobionic sensor can be used to monitor arsenite levels well below the  
311 regulatory limit of arsenic in drinking water ( $10 \text{ ppb}$ ) and in irrigation water ( $100 \text{ ppb}$ ). This figure of  
312 merit is also lower than the detection limit of the G-SWNT nanosensor alone ( $122 \text{ nM}$ ;  $15.8 \text{ ppb}$ ),  
313 highlighting the ability of *P. cretica* to pre-concentrate and hyperaccumulate arsenite to increase the  
314 detection sensitivity of a nanobionic sensor. A lower detection limit can be achieved at longer  
315 uptake duration with a larger root biomass and a higher uptake solution volume (**Figure S9,**  
316 **Supporting Information**). When the uptake period is extended to 14 days, the detection limit of the  
317 plant nanobionic sensor can be reduced to  $1.6 \text{ nM}$  ( $0.2 \text{ ppb}$ ) with roots of  $30 \text{ g FW}$  and uptake  
318 solution volume of  $5 \text{ L}$  (**Figure 4f**). While this limit of detection may not apply to rice or spinach  
319 plants tested earlier, these species may still constitute useful plant-based sensors to monitor arsenic  
320 accumulation in heavily-contaminated areas, as well as in edible plants for food safety evaluation  
321 and plant science studies.

## 322 **Competitive inhibition of silicon on arsenite uptake in *Pteris cretica***

323 The ability of ferns in the *Pteridaceae* family to tolerate and hyperaccumulate exceptionally  
324 high levels of arsenic appears to result from the presence of certain genes and proteins recently

325 identified in *P. vittata*. Arsenite antiporter gene *ACR3* was found to be necessary for arsenic  
326 tolerance in *P. vittata* gametophytes by mediating the vacuolar sequestration of arsenite.<sup>[59]</sup>  
327 Similarly, the *GAPC1*, *GSTF1* and *OCT4* proteins are required for the import and reduction of  
328 arsenate inside the cells.<sup>[65]</sup> However, the uptake pathway of arsenite in *Pteridaceae* ferns has not  
329 been fully elucidated, partly due to the difficulty in generating transgenic ferns.<sup>[66]</sup> In rice, the uptake  
330 of arsenite into rice roots is primarily facilitated by *OsNIP2;1* (*Ls1*), a member of the nodulin-26 like  
331 intrinsic proteins (NIPs) that is also responsible for the uptake of silicon (Si).<sup>[12,67]</sup> In *P. vittata*, the  
332 aquaporin tonoplast intrinsic protein 4 (*TIP4*) is the only channel to date that has been shown to  
333 mediate arsenite uptake.<sup>[68]</sup> It is unknown if arsenite uptake in *Pteridaceae* ferns share the same  
334 pathways or transporters as those responsible for Si influx into the roots. In this study, we used the  
335 optical nanosensors to investigate the effect of Si on arsenite uptake in *P. cretica*. As expected, the  
336 fluorescence intensity of (GT)<sub>5</sub>-SWNT showed a steady increase upon exposure to 10 μM arsenite for  
337 5 hours, while that of C<sub>10</sub>-SWNT remained invariant (**Figure 5a**). The addition of silicic acid to the  
338 medium suppressed arsenite uptake by *P. cretica*, as shown by the slower and insignificant change in  
339 embedded (GT)<sub>5</sub>-SWNT intensity after 5 hours of treatment (**Figure 5a**). Image analysis showed that  
340 while the mean relative intensity of (GT)<sub>5</sub>-SWNT to C<sub>10</sub>-SWNT increased by approximately 15% after  
341 5-hour exposure to arsenite, the presence of silicic acid in the arsenite uptake medium led to  
342 negligible arsenite accumulation in *P. cretica*. To ascertain that this competitive inhibition effect can  
343 be attributed uniquely to silicic acid, the fern roots were also subjected to an uptake medium  
344 containing both arsenite and phosphate. Extensive physiological data across plant species have  
345 shown that phosphate and arsenate uptake are mediated by the same transporters.<sup>[61,69–72]</sup> The  
346 presence of phosphate did not inhibit arsenite uptake in *P. cretica* as monitored by our nanosensors  
347 (**Figure 5a**). The sensor response was similar in terms of magnitude and temporal profile to the case  
348 where only arsenite was present in the medium. The average relative intensity of (GT)<sub>5</sub>-SWNT to C<sub>10</sub>-  
349 SWNT increased by 13% after 5-hour exposure to the root uptake medium containing both  
350 phosphate and arsenite (**Figure 5b**). As an example of the novel utility of the sensors introduced in  
351 this work, these results indicate that the arsenite and Si uptake in *P. cretica* may share the same  
352 transport systems previously identified in rice.<sup>[12,73]</sup> The application of our nanosensors to investigate  
353 mechanisms of arsenite uptake in *P. cretica* further illustrates the versatility of our plant nanobionic  
354 approach, which can be utilized for the creation of a new class of sensors as well as to aid botany  
355 research.

## 356 CONCLUSIONS

357 In this work, we demonstrate the integration of nanoparticles with living plants to engineer  
358 plant nanobionic sensors capable of real-time detection of arsenite in the belowground  
359 environment. DNA-wrapped SWNT nanosensors were rationally designed using the CoPhMoRe  
360 technique for selective and sensitive arsenite detection. These nanoconstructs can be incorporated  
361 into the tissues of wild-type plants and remained sensitive in vivo, enabling the conversion of living  
362 plants into microfluidic arsenite detectors capable of autosampling their surroundings through  
363 natural transpiration. Surface modification of DNA-SWNT constructs allows the versatile use of these  
364 sensors in both the NIR and visible region for whole plant and subcellular imaging. We also showed  
365 that the sensitivity of plant nanobionic sensors can be significantly enhanced by exploiting the

366 hyperaccumulating capability of select species such as *P. cretica*. Such plants exhibit high capacity in  
367 arsenite extraction from the belowground environment and its translocation to their fronds. In  
368 addition, hyperaccumulators can tolerate high concentrations of arsenite, promoting their use as  
369 sensitive sensing devices in their natural environment. The increased sensitivity of plant nanobionic  
370 sensors compared to optical nanosensors alone illustrates the synergistic properties of plant  
371 nanobionic devices by actively pre-concentrating specific analytes *in vivo* and enabling the  
372 communication of this analyte through an optical signal easily intercepted by electronic devices. We  
373 envision that the ability of select plants to pre-concentrate and hyperaccumulate specific analytes,  
374 resulting in a much higher internal concentration without showing any signs of toxicity, can be  
375 extended to engineer other plant nanobionic sensors for environmental monitoring applications.  
376 Hyperaccumulators of other metalloids or trace elements, an extensive list of which has been  
377 compiled,<sup>[74]</sup> can be potentially converted into ultrasensitive detectors of their environment with the  
378 proposed plant nanobionic approach. The versatility of plant nanobionics was also shown through  
379 sensor application in plant science research to investigate the uptake pathways of arsenite in *P.*  
380 *cretica*. This new class of nanobionic sensors should find immediate utility in environmental  
381 monitoring and agronomic studies.

382

Author Manuscript

## 383 EXPERIMENTAL METHODS

### 384 Materials

385 All reagents were purchased from Sigma Aldrich unless otherwise stated.

### 386 Preparation of DNA-SWNT nanoconstructs

387 Raw HiPCO SWNTs were obtained from NanoIntegris (Lot #HR27-104). Single stranded DNA  
388 oligonucleotides were purchased from Integrated DNA Technologies. 1 mg of SWNT was mixed with  
389 0.25 mg of ssDNA in 1 mL of 0.1 M NaCl. The mixture was sonicated with 3 mm probe tip (Cole-  
390 Parmer) at 40% amplitude for 20 min in an ice bath. The sample was then centrifuged at 30,000 g for  
391 90 minutes to remove unsuspended SWNT aggregates. The collected supernatant was dialyzed  
392 against 0.1 M NaCl with a 20 kDa MWCO dialysis bag (Spectra-Por) for three days to remove excess  
393 ssDNA.

394 TP-(GT)<sub>5</sub>-SWNT and TP-C<sub>10</sub>-SWNT prepared according to previously published method with slight  
395 modification.<sup>[75]</sup> Briefly, 1 mg of SWNT was mixed with 0.25 mg of ssDNA and TP solution at a  
396 dye:ssDNA ratio of 1:4 in 1 mL of deionized water. Tip-sonication and centrifugation were carried as  
397 described above in DNA-SWNT nanosconstruct preparation. The collected supernatant was dialyzed  
398 against deionized water with a 20 kDa MWCO dialysis bag (Spectra-Por) for three days.

### 399 Absorption spectra measurement

400 The UV-VIS absorption spectra of DNA-SWNT and TP-labelled DNA-SWNT were collected using a  
401 quartz cuvette (Starna) with 1-cm path length in Shimadzu UV-3101PC spectrophotometer. All  
402 absorption spectra were background-subtracted using reference solutions. The concentration of the  
403 DNA-SWNT nanosensors was determined using its absorbance at 632 nm and extinction coefficient  
404 of 0.036 L mg<sup>-1</sup> cm<sup>-1</sup>.

### 405 Plant growth

406 Seeds of carmel spinach (*Spinacia oleracea*) were purchased from David's Garden Seeds. Seeds of  
407 *indica* rice cultivar (*Oryza sativa*; IR24) were kindly donated by Professor Bing Yang laboratory  
408 (Donald Danforth Plant Science Center, St. Louis, MO). Cretan brake fern (*Pteris cretica*) plants were  
409 obtained from Josh's Frogs. Plant seeds were grown in Fafard Professional all-purpose blend potting  
410 soil in a Conviron Adaptis 1000 growth chamber. Spinach plants and Cretan brake ferns were grown  
411 with a 14-h-light/10-h-dark photoperiod at 100 μmol s<sup>-1</sup> m<sup>-2</sup>, 60% relative humidity, and day/night  
412 temperatures of 22 and 18°C respectively. Rice seeds were first germinated at 37°C for 4 days. Rice  
413 seedlings were then washed carefully with water and transplanted to potting soils in growth  
414 chamber with 12-h-light/12-h-dark photoperiod at 100 μmol s<sup>-1</sup> m<sup>-2</sup>, 60% relative humidity, and  
415 day/night temperature of 28 and 25°C respectively. Fertilizer (N:P:K = 15:9:12) was applied to the  
416 potting soil every two weeks.

### 417 Nanosensor screening and selectivity test

418 DNA-SWNT nanoconstructs were diluted with 0.1 M NaCl, MES buffer (10 mM MES, 10 mM MgCl<sub>2</sub>,  
419 pH 5.7), or TES buffer (10 mM TES, 10 mM MgCl<sub>2</sub>, pH 7.5) to a concentration of 2 mg L<sup>-1</sup>. Aliquots of  
420 SWNT suspensions were added to a 96-well plate for high-throughput screening. The fluorescence  
421 spectra of DNA-SWNT complexes were recorded with a custom-made NIR microscope array before  
422 and after a 30-minute incubation of SWNT aliquots with 100 μM heavy metal cations. Briefly, the 96-  
423 well plate was mounted on a motorized stage of a Zeiss AxioVision inverted microscope connected  
424 to a 1D InGaAs detector (Princeton instruments) with a PI Acton SP2500 spectrometer. The samples  
425 were excited with a 785-nm photodiode laser (Invictus) at the sample plane with x20 objective for a  
426 10-s exposure time. The fluorescence intensity at 1128 nm wavelength, corresponding to the (9,4)  
427 chirality, was used to compare the sensor selectivity and response  $((I-I_0)/I_0)$ , where  $I_0$  is the initial  
428 fluorescence intensity before analyte addition and  $I$  is the fluorescence intensity after analyte  
429 addition. The sensor responses of TP-(GT)<sub>5</sub>-SWNT and TP-C<sub>10</sub>-SWNT was measured in the NIR range  
430 using the method described above, and in the visible range using a Varioskan Flash microplate  
431 reader (Thermo Scientific). The fluorescence intensity corresponding to the maximum fluorescence  
432 peak at 540 nm was used to obtain the visible sensor response.

### 433 **Nanosensor infiltration and standoff imaging of arsenite uptake**

434 Spinach, rice and fern plants were infiltrated with both (GT)<sub>5</sub>-SWNT and C<sub>10</sub>-SWNT, which were  
435 prepared at 5 mg L<sup>-1</sup> concentration in MES buffer. Gentle pressure was applied to the abaxial side of  
436 the leaf to ensure no damage was inflicted during the needleless syringe infiltration of the  
437 nanosensors. For rice, a small puncture was introduced to the leaf surface using a pipette tip, after  
438 which DNA-SWNT was infiltrated through the puncture with a gentle pressure during syringe  
439 infiltration. The nanosensors were infiltrated to opposite sides of the leaf midrib. The plant roots  
440 were then washed with deionized water carefully to remove the soils and transferred to a  
441 pretreatment solution containing 10 mM KCl and 5 mM MES of pH 6.0. A 785 nm laser was used to  
442 excite the embedded DNA-SWNT complexes. The NIR fluorescence intensity of both sensors were  
443 spatiotemporally monitored at a standoff distance of 1 m with a 2D InGaAs array (Princeton  
444 Instruments OMA V) equipped with a Nikon AF Micro-Nikkor 60 mm f/2.8D lens. Images were  
445 collected at a 2-second exposure time unless otherwise stated. A 900 nm long-pass filter was placed  
446 in front of the camera lens to eliminate chlorophyll autofluorescence and the reflected excitation  
447 beam. After 20 minutes, the pretreatment solution incubating the roots was then replaced with a  
448 solution containing 10 μM or 0.1 μM of sodium meta-arsenite (NaAsO<sub>2</sub>) unless otherwise stated.

449 For 7-day experiments, 10 images were taken daily at a specific time during the day and the  
450 fluorescence intensity was averaged from the 10 images for a daily profile. The excitation laser was  
451 turned off when images were not collected. Roots of treated plants were weighed to obtain their  
452 fresh weights. To calibrate the nanosensor fluorescence intensities in *Pteris cretica*, the frond arsenic  
453 concentration was analyzed with ICP-MS by Galbraith Laboratories Inc. (Knoxville, TN). Briefly, frond  
454 samples were cut at specific time points after arsenite treatment, rinsed with deionized water and  
455 dried at 60°C for 48 hours. They were then weighed, ground to fine powder and analyzed by ICP-MS.

### 456 **Image and data analysis**

457 Image and data analysis were performed with ImageJ and Matlab R2018a. The sensor response was  
458 obtained from imaging experiments by normalizing the SWNT fluorescence with the corresponding  
459 initial value prior to the introduction of arsenite. 100 brightest pixels in a sensor spot were averaged  
460 to obtain a mean fluorescence intensity value. The normalized (GT)<sub>5</sub>-SWNT intensity profile was  
461 divided with that of C<sub>10</sub>-SWNT to yield a ratiometric sensor profile ( $I_{G/C-SWNT}$ ). In Figure 4, the change  
462 in ratiometric sensor profile relative to the initial value is denoted as  $\Delta I/I_0$ . Snapshots of false-colored  
463 images were generated by subtracting the first image collected at the time point of arsenite  
464 introduction from subsequent images. Numerical simulation of the kinetic model to fit arsenite  
465 concentration profile in *Pteris cretica* was performed with *ode45* solver in Matlab R2018a. The  
466 sensor limit of detection was also simulated using Matlab R2018a.

467 **Confocal microscopy**

468 Confocal images were obtained using a Zeiss LSM 710 microscope. 20  $\mu\text{L}$  of TP-(GT)<sub>5</sub>-SWNT in MES  
469 buffer was infiltrated into spinach leaves as attached to living plants. The leaf was excised 1 hour  
470 after infiltration and a leaf disc (5 mm) was prepared using a cork borer. The leaf disc was then  
471 transferred to a glass slide with a polydimethylsiloxane (PDMS) chamber filled with water. The  
472 chamber was sealed with a cover slip and imaged with a 40x water-immersion objective. A final  
473 concentration of 10  $\mu\text{M}$  arsenite solution was introduced into the chamber medium from the side of  
474 the cover slip with a pipette. TP-(GT)<sub>5</sub>-SWNT nanosensors were excited with a 514 nm laser with  
475 emission channel from 530 to 570 nm. Chlorophyll autofluorescence imaging was obtained by  
476 excitation at 633 nm with emission channel between 660 and 750 nm. Confocal images of TP-(GT)<sub>5</sub>-  
477 SWNT and chloroplast autofluorescence were captured every 5 minutes.

478 **Silicon, phosphate and arsenite interaction experiments**

479 *Pteris cretica* plants were used in these experiments. The roots of the plants were gently removed  
480 from the soil and carefully washed with water. The plants were then transferred to a beaker  
481 containing a pretreatment solution of 10 mM KCl and 5 mM MES at pH 6.0. After nanosensor  
482 infiltration, plants were incubated in the growth chamber for 1 hour before imaging. At the start of  
483 the experiments, the pretreatment solution was replaced with solutions containing 10  $\mu\text{M}$  arsenite,  
484 10  $\mu\text{M}$  arsenite and 100  $\mu\text{M}$  phosphate (supplied as  $\text{KH}_2\text{PO}_4$ ), or 10  $\mu\text{M}$  arsenite and 100  $\mu\text{M}$  silicic  
485 acid which was prepared from  $\text{SiO}_2$  according to a previously published method.<sup>[76]</sup>



486 **ACKNOWLEDGEMENTS**

487 This research was supported by the National Research Foundation (NRF), Prime Minister's Office,  
488 Singapore under its Campus for Research Excellence and Technological Enterprise (CREATE)  
489 program. The Disruptive & Sustainable Technology for Agricultural Precision (DiSTAP) is an  
490 interdisciplinary research group of the Singapore MIT Alliance for Research and Technology  
491 (SMART) Centre. T.T.S.L. was supported on a graduate fellowship by the Agency of Science,  
492 Research and Technology, Singapore. The authors would like to thank N.-H. Chua and Z. Yin from  
493 Temasek Life Sciences Laboratory, Singapore for useful discussions.

494 **AUTHOR INFORMATION**

495 **Corresponding Author**

496 \*E-mail: strano@mit.edu. Phone: 617.324.4323. Fax: 617.258.8824.

497 **ORCID**

498 Tedrick Thomas Salim Lew: 0000-0002-4815-9921

499 Michael S. Strano: 0000-0003-2944-808X

500 **Author Contributions**

501 T.T.S.L. and M.S.S. conceived the project, designed the study and wrote the manuscript. M.P. and  
502 J.C. assisted with data analysis and nanoparticle characterization.

503 **Competing interests**

504 The authors declare no competing interest.

Author Manuscript

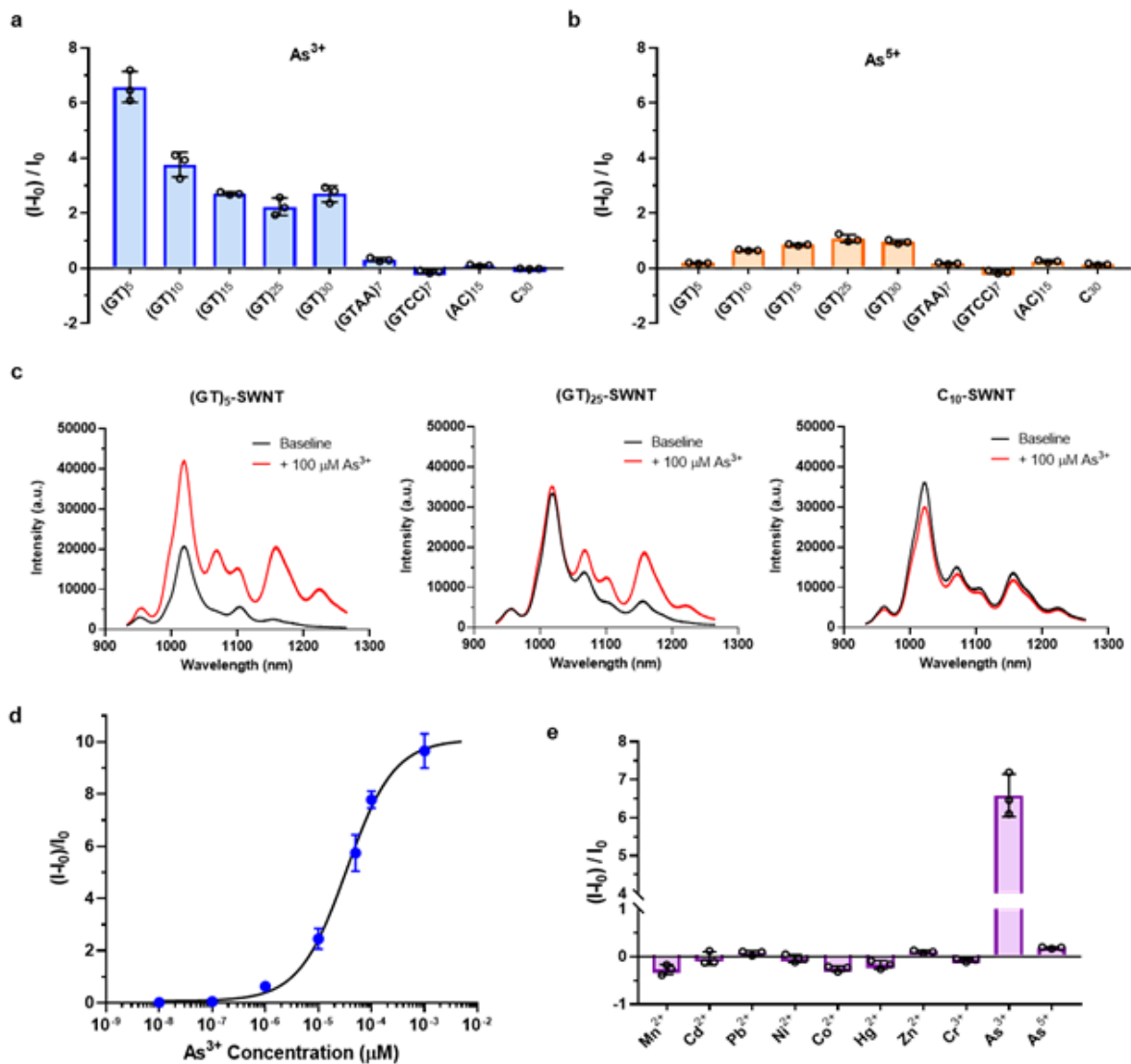
505 **References**

- 506 [1] A. H. Smith, P. A. Lopipero, M. N. Bates, C. M. Steinmaus, *Science* (80-. ). **2002**, 296, 2145.  
 507 [2] H. Brammer, P. Ravenscroft, *Environ. Int.* **2009**, 35, 647.  
 508 [3] M. Argos, T. Kalra, P. J. Rathouz, Y. Chen, B. Pierce, F. Parvez, T. Islam, A. Ahmed, M. Rakibuz-  
 509 Zaman, R. Hasan, G. Sarwar, V. Slavkovich, A. Van Geen, J. Graziano, H. Ahsan, *Lancet* **2010**,  
 510 376, 252.  
 511 [4] K. S. Mohammed Abdul, S. S. Jayasinghe, E. P. S. Chandana, C. Jayasumana, P. M. C. S. De  
 512 Silva, *Environ. Toxicol. Pharmacol.* **2015**, 40, 828.  
 513 [5] R. Singh, S. Singh, P. Parihar, V. P. Singh, S. M. Prasad, *Ecotoxicol. Environ. Saf.* **2015**, 112, 247.  
 514 [6] S. Quazi, D. Sarkar, R. Datta, *J. Hazard. Mater.* **2013**, 262, 1031.  
 515 [7] R. Q. Huang, S. F. Gao, W. L. Wang, S. Staunton, G. Wang, *Sci. Total Environ.* **2006**, 368, 531.  
 516 [8] E. M. Muehe, T. Wang, C. F. Kerl, B. Planer-Friedrich, S. Fendorf, *Nat. Commun.* **2019**, 10, 1.  
 517 [9] A. L. Seyfferth, S. McCurdy, M. V. Schaefer, S. Fendorf, *Environ. Sci. Technol.* **2014**, 48, 4699.  
 518 [10] N. US EPA, OCSPP, OPPT, "Chemical Contaminant Rules \_ Drinking Water Requirements for  
 519 States and Public Water Systems \_ US EPA," can be found under  
 520 <https://www.epa.gov/dwreginfo/chemical-contaminant-rules>, **2016**.  
 521 [11] D. E. Mays, A. Hussam, *Anal. Chim. Acta* **2009**, 646, 6.  
 522 [12] F. M. Jian, N. Yamaji, N. Mitani, X. Y. Xu, Y. H. Su, S. P. McGrath, F. J. Zhao, *Proc. Natl. Acad.*  
 523 *Sci. U. S. A.* **2008**, 105, 9931.  
 524 [13] W. Y. Song, T. Yamaki, N. Yamaji, D. Ko, K. H. Jung, M. Fujii-Kashino, G. An, E. Martinoia, Y.  
 525 Lee, J. Feng, *Proc. Natl. Acad. Sci. U. S. A.* **2014**, 111, 15699.  
 526 [14] A. H. Ackerman, P. A. Creed, A. N. Parks, M. W. Fricke, C. A. Schwegel, J. T. Creed, D. T.  
 527 Heitkemper, N. P. Vela, *Environ. Sci. Technol.* **2005**, 39, 5241.  
 528 [15] D. Melamed, *Anal. Chim. Acta* **2005**, 532, 1.  
 529 [16] E. Durduran, H. Altundag, M. Imamoglu, S. Z. Yildiz, M. Tuzen, *J. Ind. Eng. Chem.* **2015**, 27,  
 530 245.  
 531 [17] J. Mattusch, R. Wennrich, A. C. Schmidt, W. Reisser, *Fresenius. J. Anal. Chem.* **2000**, 366, 200.  
 532 [18] D. K. Gupta, S. Chatterjee, *Arsen. Contam. Environ. Issues Solut.* **2017**, 1.  
 533 [19] T. Shi, H. Liu, J. Wang, Y. Chen, T. Fei, G. Wu, *Environ. Sci. Technol.* **2014**, 48, 6264.  
 534 [20] V. Bandaru, C. Daughtry, E. Codling, D. Hansen, S. White-Hansen, C. Green, *Int. J. Environ. Res.*  
 535 *Public Health* **2016**, 13, 606.  
 536 [21] X. Li, X. Liu, M. Liu, C. Wang, X. Xia, *Int. J. Appl. Earth Obs. Geoinf.* **2015**, 36, 41.  
 537 [22] W. Zhou, J. Zhang, M. Zou, X. Liu, X. Du, Q. Wang, Y. Liu, Y. Liu, J. Li, *Sci. Rep.* **2019**, 9, 1.  
 538 [23] K. Mao, H. Zhang, Z. Wang, H. Cao, K. Zhang, X. Li, Z. Yang, *Biosens. Bioelectron.* **2020**, 148,  
 539 111785.  
 540 [24] P. Devi, A. Thakur, R. Y. Lai, S. Saini, R. Jain, P. Kumar, *TrAC - Trends Anal. Chem.* **2019**, 110,  
 541 97.  
 542 [25] L. Cui, J. Wu, H. Ju, *Biosens. Bioelectron.* **2016**, 79, 861.  
 543 [26] K. Matsunaga, Y. Okuyama, R. Hirano, S. Okabe, M. Takahashi, H. Satoh, *Chemosphere* **2019**,  
 544 224, 538.  
 545 [27] S. H. Wen, Y. Wang, Y. H. Yuan, R. P. Liang, J. D. Qiu, *Anal. Chim. Acta* **2018**, 1002, 82.  
 546 [28] J. Zhang, M. P. Landry, P. W. Barone, J. H. Kim, S. Lin, Z. W. Ulissi, D. Lin, B. Mu, A. A.  
 547 Boghossian, A. J. Hilmer, A. Rwei, A. C. Hinckley, S. Kruss, M. A. Shandell, N. Nair, S. Blake, F.  
 548 Sen, S. Sen, R. G. Croy, D. Li, K. Yum, J. H. Ahn, H. Jin, D. A. Heller, J. M. Essigmann, D.  
 549 Blankshtein, M. S. Strano, *Nat. Nanotechnol.* **2013**, 8, 959.  
 550 [29] J. P. Giraldo, M. P. Landry, S. M. Faltermeier, T. P. McNicholas, N. M. Iverson, A. A.  
 551 Boghossian, N. F. Reuel, A. J. Hilmer, F. Sen, J. A. Brew, M. S. Strano, *Nat. Mater.* **2014**, 13,  
 552 400.

- 553 [30] M. H. Wong, J. P. Giraldo, S. Y. Kwak, V. B. Koman, R. Sinclair, T. T. S. Lew, G. Bisker, P. W. Liu,  
554 M. S. Strano, *Nat. Mater.* **2017**, *16*, 264.
- 555 [31] T. T. S. Lew, V. B. Koman, K. S. Silmore, J. S. Seo, P. Gordiichuk, S.-Y. Kwak, M. Park, M. C.-Y.  
556 Ang, D. T. Khong, M. A. Lee, M. B. Chan-Park, N.-H. Chua, M. S. Strano, *Nat. Plants* **2020**, *6*,  
557 404.
- 558 [32] S.-Y. Kwak, M. H. Wong, T. T. S. Lew, G. Bisker, M. A. Lee, A. Kaplan, J. Dong, A. T. Liu, V. B.  
559 Koman, R. Sinclair, C. Hamann, M. S. Strano, *Annu. Rev. Anal. Chem.* **2017**, *10*, 113.
- 560 [33] T. T. S. Lew, V. B. Koman, P. Gordiichuk, M. Park, M. S. Strano, *Adv. Mater. Technol.* **2020**, *5*,  
561 1900657.
- 562 [34] T. T. S. Lew, M. H. Wong, S. Y. Kwak, R. Sinclair, V. B. Koman, M. S. Strano, *Small* **2018**, *14*,  
563 1802086.
- 564 [35] S. Y. Kwak, T. T. S. Lew, C. J. Sweeney, V. B. Koman, M. H. Wong, K. Bohmert-Tatarev, K. D.  
565 Snell, J. S. Seo, N. H. Chua, M. S. Strano, *Nat. Nanotechnol.* **2019**, *14*, 447.
- 566 [36] T. T. S. Lew, M. Park, Y. Wang, P. Gordiichuk, W.-C. Yeap, S. K. Mohd Rais, H.  
567 Kulaveerasingam, M. S. Strano, *ACS Mater. Lett.* **2020**, *2*, 1057.
- 568 [37] Y. Takahashi, R. Minamikawa, K. H. Hattori, K. Kurishima, N. Kihou, K. Yuita, *Environ. Sci.*  
569 *Technol.* **2004**, *38*, 1038.
- 570 [38] N. Li, J. Wang, W.-Y. Song, *Plant Cell Physiol.* **2016**, *57*, 4.
- 571 [39] S. Nafisi, A. Sobhanmanesh, K. Alimoghaddam, A. Ghavamzadeh, H. A. Tajmir-Riahi, *DNA Cell*  
572 *Biol.* **2005**, *24*, 634.
- 573 [40] L. Zhang, X. Z. Cheng, L. Kuang, A. Z. Xu, R. P. Liang, J. D. Qiu, *Biosens. Bioelectron.* **2017**, *94*,  
574 701.
- 575 [41] A. G. Beyene, A. A. Alizadehmojarad, G. Dorlhiac, N. Goh, A. M. Streets, P. Král, L. Vuković, M.  
576 P. Landry, *Nano Lett.* **2018**, *18*, 6995.
- 577 [42] M. Zheng, A. Jagota, M. S. Strano, A. P. Santos, P. Barone, S. G. Chou, B. A. Diner, M. S.  
578 Dresselhaus, R. S. McLean, G. B. Onoa, G. G. Samsonidze, E. D. Semke, M. Usrey, D. J. Watts,  
579 *Science (80-. )*. **2003**, *302*, 1545.
- 580 [43] Y. Wu, S. Zhan, F. Wang, L. He, W. Zhi, P. Zhou, *Chem. Commun.* **2012**, *48*, 4459.
- 581 [44] M. P. Landry, L. Vuković, S. Kruss, G. Bisker, A. M. Landry, S. Islam, R. Jain, K. Schulten, M. S.  
582 Strano, *J. Phys. Chem. C* **2015**, *119*, 10048.
- 583 [45] D. P. Salem, X. Gong, A. T. Liu, V. B. Koman, J. Dong, M. S. Strano, *J. Am. Chem. Soc.* **2017**, *139*,  
584 16791.
- 585 [46] D. P. Salem, M. P. Landry, G. Bisker, J. Ahn, S. Kruss, M. S. Strano, *Carbon N. Y.* **2016**, *97*, 147.
- 586 [47] G. M. Newkirk, H. Wu, I. Santana, J. P. Giraldo, *J. Vis. Exp.* **2018**, *2018*, 58373.
- 587 [48] S. Kruss, M. P. Landry, E. Vander Ende, B. M. A. Lima, N. F. Reuel, J. Zhang, J. Nelson, B. Mu, A.  
588 Hilmer, M. Strano, *J. Am. Chem. Soc.* **2014**, *136*, 713.
- 589 [49] Y. G. Zhu, G. X. Sun, M. Lei, M. Teng, Y. X. Liu, N. C. Chen, L. H. Wang, A. M. Carey, C. Deacon,  
590 A. Raab, A. A. Meharg, P. N. Williams, *Environ. Sci. Technol.* **2008**, *42*, 5008.
- 591 [50] H. F. Bakhat, Z. Zia, S. Fahad, S. Abbas, H. M. Hammad, A. N. Shahzad, F. Abbas, H. Alharby,  
592 M. Shahid, *Environ. Sci. Pollut. Res.* **2017**, *24*, 9142.
- 593 [51] P. N. Williams, A. Villada, C. Deacon, A. Raab, J. Figuerola, A. J. Green, J. Feldmann, A. A.  
594 Meharg, *Environ. Sci. Technol.* **2007**, *41*, 6854.
- 595 [52] Y. H. Su, S. P. McGrath, F. J. Zhao, *Plant Soil* **2010**, *328*, 27.
- 596 [53] G. L. Silva, V. Ediz, D. Yaron, B. A. Armitage, *J. Am. Chem. Soc.* **2007**, *129*, 5710.
- 597 [54] A. A. Meharg, *New Phytol.* **2003**, *157*, 25.
- 598 [55] M. Srivastava, L. Q. Ma, J. A. G. Santos, *Sci. Total Environ.* **2006**, *364*, 24.
- 599 [56] Z. Sourì, N. Karimi, L. M. Sandalio, *Front. Cell Dev. Biol.* **2017**, *5*, DOI  
600 10.3389/fcell.2017.00067.

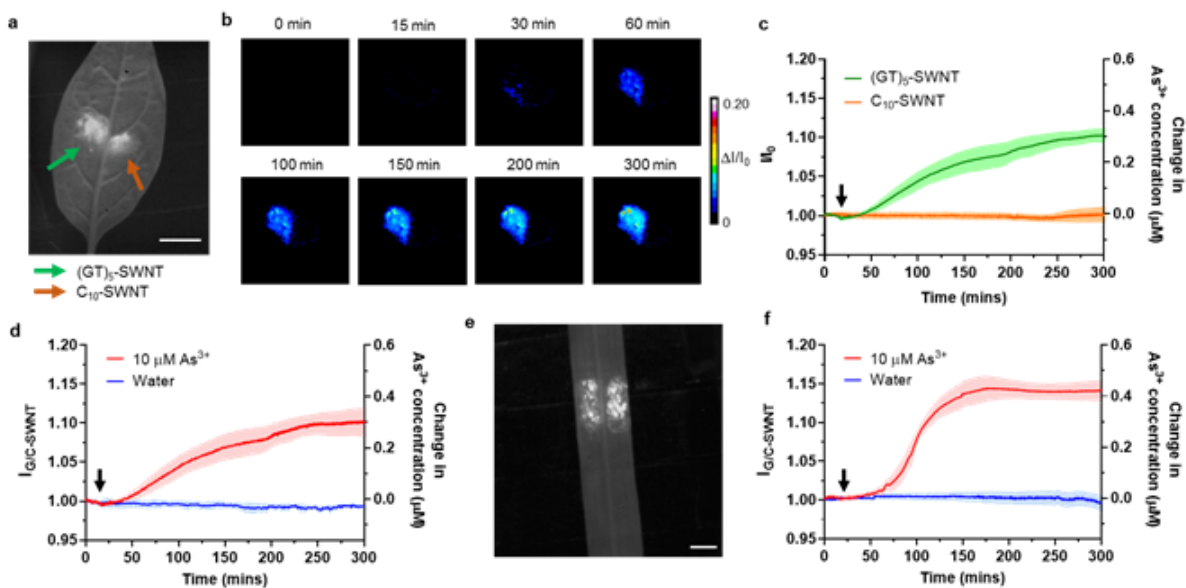
- 601 [57] L. Q. Ma, K. M. Komar, C. Tu, W. Zhang, Y. Cai, E. D. Kennelley, *Nature* **2001**, 409, 579.  
602 [58] S. Jeong, H. S. Moon, K. Nam, *J. Hazard. Mater.* **2014**, 280, 536.  
603 [59] E. Indriolo, G. N. Na, D. Ellis, D. E. Salt, J. A. Banks, *Plant Cell* **2010**, 22, 2045.  
604 [60] H. Shen, Z. He, H. Yan, Z. Xing, Y. Chen, W. Xu, W. Xu, M. Ma, *J. Proteomics* **2014**, 105, 46.  
605 [61] J. Wang, F. J. Zhao, A. A. Meharg, A. Raab, J. Feldmann, S. P. McGrath, *Plant Physiol.* **2002**,  
606 130, 1552.  
607 [62] X. Wan, M. Lei, T. Chen, J. Yang, H. Liu, Y. Chen, *Environ. Sci. Pollut. Res.* **2015**, 22, 16631.  
608 [63] Y. H. Su, S. P. McGrath, Y. G. Zhu, F. J. Zhao, *New Phytol.* **2008**, 180, 434.  
609 [64] A. A. Meharg, L. Jardine, *New Phytol.* **2003**, 157, 39.  
610 [65] C. Cai, N. A. Lanman, K. A. Withers, A. M. DeLeon, Q. Wu, M. Gribskov, D. E. Salt, J. A. Banks,  
611 *Curr. Biol.* **2019**, 29, 1625.  
612 [66] B. Muthukumar, B. L. Joyce, M. P. Elless, C. N. Stewart, *Plant Physiol.* **2013**, 163, 648.  
613 [67] J. F. Ma, N. Yamaji, *Trends Plant Sci.* **2006**, 11, 392.  
614 [68] Z. He, H. Yan, Y. Chen, H. Shen, W. Xu, H. Zhang, L. Shi, Y. G. Zhu, M. Ma, *New Phytol.* **2016**,  
615 209, 746.  
616 [69] Y. G. Zhu, C. N. Geng, Y. P. Tong, S. E. Smith, F. A. Smith, *Ann. Bot.* **2006**, 98, 631.  
617 [70] S. F. DiTusa, E. B. Fontenot, R. W. Wallace, M. A. Silvers, T. N. Steele, A. H. Elnagar, K. M.  
618 Dearman, A. P. Smith, *New Phytol.* **2016**, 209, 762.  
619 [71] A. A. Meharg, J. Hartley-Whitaker, *New Phytol.* **2002**, 154, 29.  
620 [72] G. T. Clark, J. Dunlop, H. T. Phung, *Aust. J. Plant Physiol.* **2000**, 27, 959.  
621 [73] F. J. Zhao, J. F. Ma, A. A. Meharg, S. P. McGrath, *New Phytol.* **2009**, 181, 777.  
622 [74] R. D. Reeves, A. J. M. Baker, T. Jaffré, P. D. Erskine, G. Echevarria, A. van der Ent, *New Phytol.*  
623 **2018**, 218, 407.  
624 [75] O. Cavuslar, H. Unal, *RSC Adv.* **2015**, 5, 22380.  
625 [76] X. Gao, R. A. Root, J. Farrell, W. Ela, J. Chorover, *Appl. Geochemistry* **2013**, 38, 110.  
626 [77] F. Wu, D. Deng, S. Wu, X. Lin, M. H. Wong, *Environ. Sci. Pollut. Res.* **2015**, 22, 8911.  
627 [78] X. Wang, L. Q. Ma, B. Rathinasabapathi, Y. Cai, Y. Guo Liu, G. Ming Zeng, *Environ. Sci. Technol.*  
628 **2011**, 45, 9719.  
629  
630

Author Manuscript



632

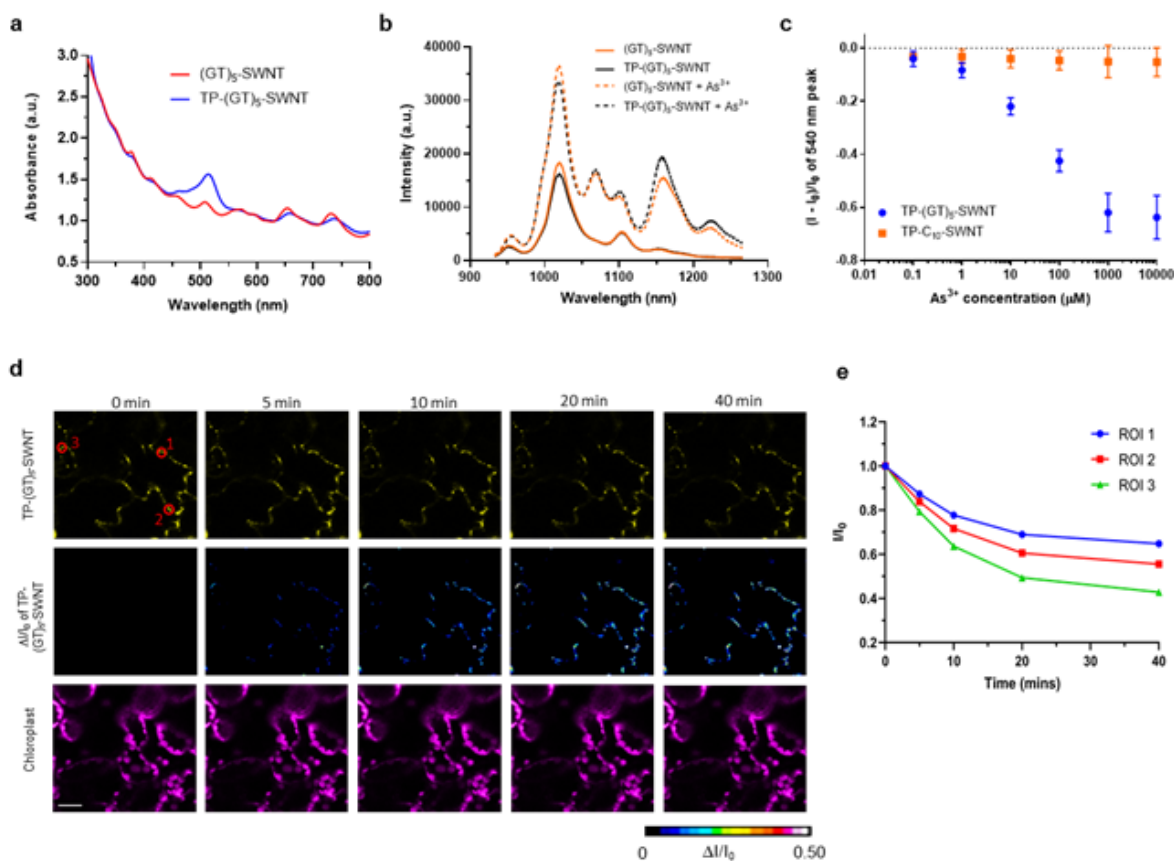
633 **Figure 1. Screening and characterization of SWNT-based arsenite sensors.** a) Comparison of sensor  
 634 responses  $(I-I_0)/I_0$  of  $(GT)_N$ -SWNT, where  $N = 5$  to  $30$ , and other DNA-SWNT constructs against  
 635 arsenite. Data represent mean  $\pm$  s.d. from  $n = 3$  independent experiments. b) DNA-SWNT responses  
 636 towards arsenate. Data represent mean  $\pm$  s.d. from  $n = 3$  independent experiments. c) NIR  
 637 fluorescence spectra of  $(GT)_5$ -SWNT,  $(GT)_{25}$ -SWNT and  $C_{10}$ -SWNT before and after exposure to  $100$   
 638  $\mu M$  arsenite. d) Calibration curve of  $(GT)_5$ -SWNT against different concentrations of arsenite. Fitting  
 639 with kinetic adsorption model is shown in black. e) Selectivity of  $(GT)_5$ -SWNT against other heavy  
 640 metal cations commonly present in the soil or groundwater. Data represent mean  $\pm$  s.d. from  $n = 3$   
 641 independent experiments.



642

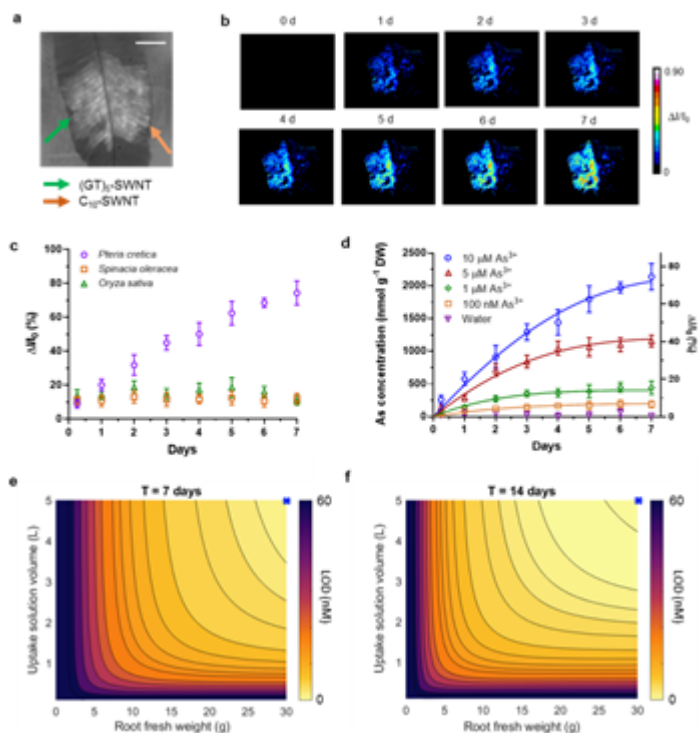
643 **Figure 2. Standoff detection of arsenite introduced via root uptake in spinach and rice plants. a)**  
 644 Brightfield image of spinach leaf infiltrated with (GT)<sub>5</sub>-SWNT and C<sub>10</sub>-SWNT under 785-nm excitation. Scale bar, 0.5 mm. b) Screenshots of false-colored images showing the change in fluorescence  
 645 intensity of embedded (GT)<sub>5</sub>-SWNT and C<sub>10</sub>-SWNT after exposure to arsenite. Time label denotes the  
 646 time points after the introduction of arsenite. c) Normalized intensity profile of (GT)<sub>5</sub>-SWNT and C<sub>10</sub>-  
 647 SWNT embedded in spinach plants upon exposure to 10 µM arsenite root medium. Shaded region  
 648 represents s.e.m. from n = 5 independent biological samples. Black arrow denotes the time point of  
 649 arsenite introduction. d) Time profile of ratiometric sensor upon spinach plant exposure to arsenite  
 650 and deionized water in the root medium. Shaded region represents s.e.m. from n = 5 independent  
 651 biological samples. Black arrow denotes the time point of arsenite introduction. e) Brightfield image  
 652 of rice blade infiltrated with (GT)<sub>5</sub>-SWNT and C<sub>10</sub>-SWNT under 785-nm excitation. Scale bar, 0.5 mm.  
 653 f) Time profile of ratiometric sensor upon rice plant exposure to arsenite and deionized water in the  
 654 root medium. Shaded region represents s.e.m. from n = 5 independent biological samples. Black  
 655 arrow denotes the time point of arsenite introduction.  
 656

Author



657

658 **Figure 3. Sensor characterization and application of TP-(GT)<sub>5</sub>-SWNT constructs in confocal imaging**  
 659 **of arsenite accumulation.** a) Absorbance spectra of (GT)<sub>5</sub>-SWNT and TP-(GT)<sub>5</sub>-SWNT confirm the  
 660 successful conjugation of TP dye as shown by the presence of the 515 nm peak. b) NIR spectra of  
 661 (GT)<sub>5</sub>-SWNT and TP-(GT)<sub>5</sub>-SWNT before and after 100 μM arsenite exposure. c) Changes in the  
 662 fluorescence of TP-(GT)<sub>5</sub>-SWNT and TP-C<sub>10</sub>-SWNT upon arsenite exposure as measured by the  
 663 emission intensity at 540 nm. Data represent mean ± s.d. from n = 3 independent experiments. d)  
 664 Confocal images capturing the spatial and temporal profile of TP-(GT)<sub>5</sub>-SWNT in the mesophyll cell of  
 665 spinach leaf lamina exposed to arsenite. Changes in the fluorescence intensity ( $\Delta I/I_0$ ) of TP-(GT)<sub>5</sub>-  
 666 SWNT were false-colored for clarity. Scale bar, 10 μm. e) Fluorescence time profile of 3 randomly  
 667 selected regions of interest (ROI) containing TP-(GT)<sub>5</sub>-SWNT corresponding to circled areas in (d)  
 668 after arsenite exposure.

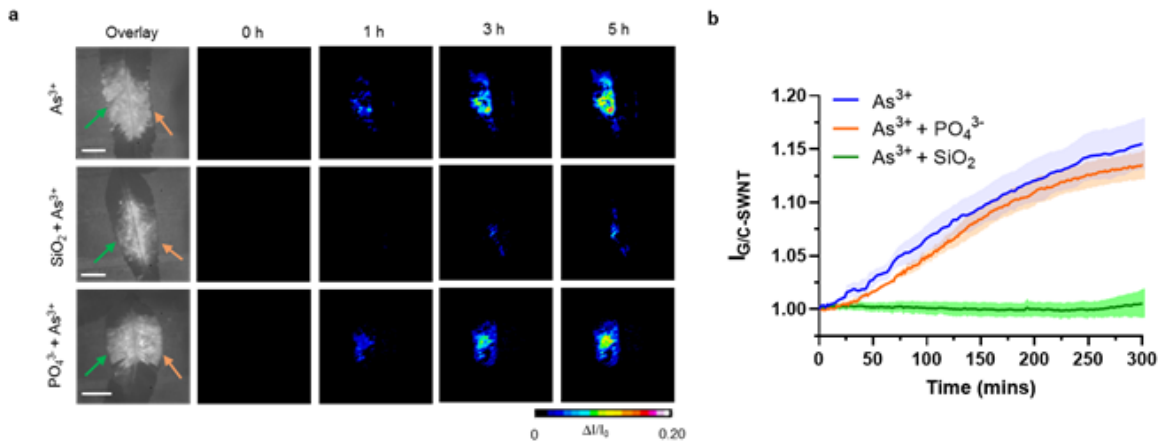


669

670 **Figure 4. Arsenite detection with nanobionic sensor based on arsenic hyperaccumulator *Pteris***  
 671 ***cretica*.** a) Brightfield image of *Pteris cretica* frond infiltrated with (GT)<sub>5</sub>-SWNT and C<sub>10</sub>-SWNT under  
 672 785-nm excitation. Scale bar, 0.5 mm. b) Time lapse images showing the intensity changes of  
 673 embedded nanosensors upon arsenite exposure. Time denotes the time points after arsenite  
 674 introduction via root uptake. c) Fluorescence intensity changes of SWNT nanosensors embedded in  
 675 spinach, rice and *Pteris cretica* plants exposed to 10 μM arsenite root medium. Data represent mean  
 676 ± s.e.m. from n = 5 independent biological samples. d) Arsenite concentration in *Pteris cretica* frond  
 677 treated with 10 μM, 5 μM, 1 μM, 0.1 μM arsenite solution and deionized water in the root medium.  
 678 The concentrations in nmol g<sup>-1</sup> DW are translated from sensor intensity responses. Data represent  
 679 mean ± s.e.m. from n = 5 independent biological samples. e) Contour plot of plant nanobionic  
 680 sensor's limit of detection as a function of uptake solution volume and root fresh weight after 7  
 681 days. Cross indicates the minimum detection limit of 4.7 nM (0.6 ppb). f) Contour plot of plant  
 682 nanobionic sensor's limit of detection as a function of uptake solution volume and root fresh weight  
 683 after 14 days. Cross indicates the minimum detection limit of 1.6 nM (0.2 ppb).

684





685

686 **Figure 5. Application of nanosensors to investigate the arsenite uptake pathway in *Pteris cretica*.**  
 687 a) False-colored images showing the embedded nanosensor response upon the exposure of *Pteris*  
 688 *cretica* roots to medium containing only arsenite, arsenite and silica, or arsenite and phosphate.  
 689 Green and orange arrows correspond to (GT)<sub>5</sub>-SWNT and C<sub>10</sub>-SWNT respectively. Scale bars, 0.5 mm.  
 690 b) Time profile of normalized nanosensor intensity upon exposure to the different root media.  
 691 Shaded region represents s.e.m. from n = 5 independent biological samples.

Author Manuscript

692 **Table 1.** Kinetic parameters estimated from the time profile of arsenite uptake in *Pteris cretica*  
 693 reported by nanosensors. Values obtained from model fitting are in agreement with reported values  
 694 from previously published reports.

Kinetic parameters	Fitting values	Reported values <sup>a</sup>	References
$K_{M_s}$ ( $\mu\text{M}$ )	$5.84 \pm 1.63$	6 - 25	[77,78]
$I_{max}$ ( $\text{nmol g}^{-1}$ root FW $\text{h}^{-1}$ )	$3.35 \pm 1.02$	8 - 10	[61]
$k_d$ ( $\text{h}^{-1}$ )	$(1.23 \pm 0.42) \times 10^{-3}$	N.A.	

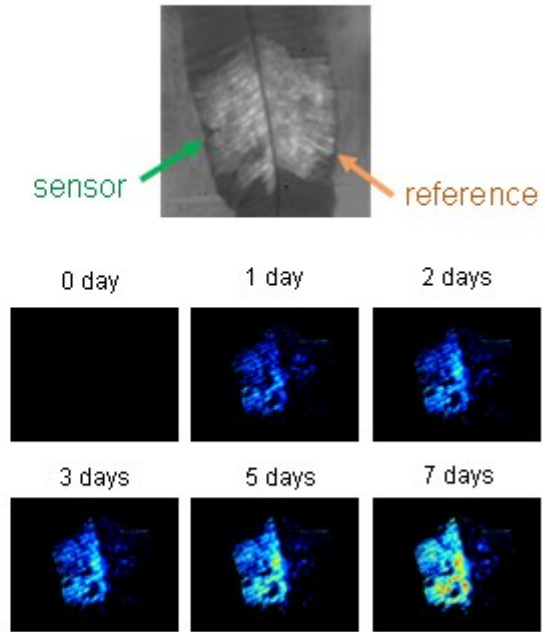
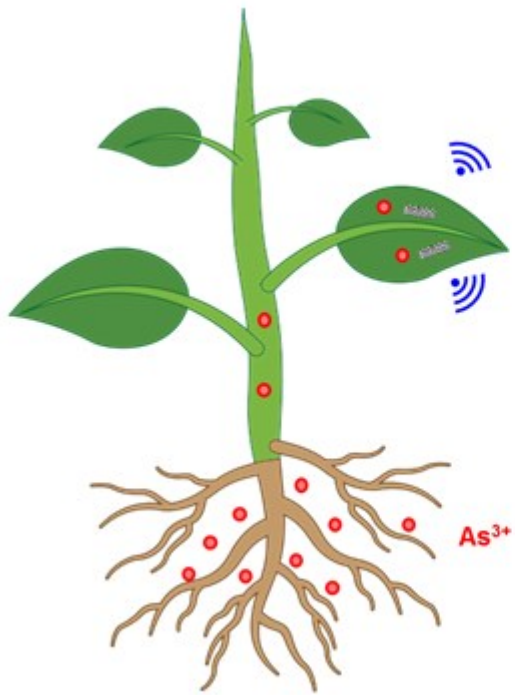
695 <sup>a</sup>Reported values were based on kinetic data on *Pteris vittata* plants.

696 ToC Text:

697

698 Exploiting the natural ability of plants to pre-concentrate and extract arsenite from the belowground  
 699 environment, a living plant nanobionic sensor is engineered for non-destructive arsenite monitoring.  
 700 By embedding near-infrared fluorescent nanosensors within the mesophyll, living plants are  
 701 converted into environmental sensors for real-time arsenite detection. This demonstration opens  
 702 new frontiers for plant-based sensors in environmental monitoring and food safety research.

Author Manuscript



703

Author Ms